Numerical study of a passive solar still with separate condenser

A. Madhlopa[*,†] and C. Johnstone

Energy Systems Research Unit, Department of Mechanical Engineering, University of Strathclyde,
75 Montrose Street, Glasgow G1 1XJ, United Kingdom.

Abstract

A passive solar still with separate condenser has been modeled and its performance evaluated. The system has one basin in the evaporation chamber and two basins (middle and upper) in the condenser chamber, with a glass cover over the evaporator basin and an opaque condensing cover over the upper basin. The evaporator, middle and upper basins yield the first, second and third effects respectively. The top part of the condensing cover is shielded from solar radiation to keep the cover relatively cool. Water vapor from the first effect condenses under the glass cover while the remainder of it flows into the condenser, by purging and diffusion, and condenses under the liner of the middle basin. The performance of the system is evaluated and compared with that of a conventional solar still under the same meteorological conditions. Results show that the distillate productivity of the present still is 62 % higher than that of the conventional type. Purging is the most significant mode of vapor transfer from the evaporator into the condenser chamber. The first, second and third effects contribute 60, 22 and 18 % of the total distillate yield respectively. It is also found that the productivity of the solar still with separate condenser is sensitive to the absorptance of the evaporator basin liner, mass of water in the evaporator and middle basins, and wind speed. The mass of water in the upper basin has a marginal effect on distillate production. Other results are presented and discussed in detail.

Keywords: Condenser, evaporator, natural circulation, simulation, solar radiation shield

[*] Corresponding author: E-mail: amadhlopa@poly.ac.mw
[†] Permanent address: Malawi Polytechnic, P/Bag 303, Blantyre 3, Malawi.

1. Introduction

Clean water is essential for good health, which relates to socio-economic development. Nevertheless, safe drinking water is scarce, especially in the developing countries due to the limitation of financial and other resources. The quality of water can be improved through the use solar stills. This technology is suitable for exploitation in the developing countries because it is cheap and requires little maintenance [1].

A basic solar distillation system has a thin layer of water in a shallow basin, transparent cover over the water and channel for collecting the distillate. Saline water in the basin is heated by solar radiation that passes through the transparent cover and is absorbed by the bottom part of the still basin. Vapor rises from the hot water and condenses when it gets into contact with the inner surface of the transparent cover. The condensate (clean water) is collected through a channel fitted along the lower edge of the transparent cover.

In a solar still, the difference between the temperature of water and cover is the driving force of the distillation process. It influences the rate of evaporation from the surface of water in the basin to the condensing cover. However, the heat transferred from hot water to the transparent cover elevates the temperature of the cover, thereby reducing the rate of distillation in a conventional solar still (CSS). Consequently, the CSS suffers from low efficiency [2]. In view of this, many researchers have attempted to improve its performance through various modifications including use of different absorbing materials [3, 4], external condensers [5], sponge cubes [6], packed layer of glass balls in the basin and rotating shaft [7].

Based on various modifications, solar stills are broadly classified into active and passive systems [8]. In solar stills of the active variety, additional thermal energy from an external mode (such as a flat plate or concentrator collector) is supplied to the evaporator to augment the temperature of the water in the basin. Tiwari et al. [8] report that active solar stills are suitable for commercial production of distilled water. No outside heat is employed in the passive variety of solar stills. In both classes of stills, water vapor flows from the evaporator to the condensing cover by natural (convection, diffusion and purging) or forced circulation. Natural circulation does not require a blower, thereby reducing costs associated with forced circulation. This study focuses on a passive solar still with external condenser and natural circulation of water vapor from the evaporator to the condensing unit.

Several researchers have suggested improvements to the passive solar still with separate condenser and natural circulation of water vapor. Fath and Elsherbiny [9] added an external condenser to a single-slope simple still. The condenser was located in the shadow zone of the still. They found that there was an increase in the still efficiency. Fath [10] developed a double-effect solar still, with the second-effect component on the shaded side of a basin solar still. It was found that the daily distillate productivity improved. El-Bahi and Inan [5] developed a solar still with double-glazing and a separate condenser. The condenser was located on the shaded side of the evaporator. El-Bahi and Inan [11] studied a solar still with one glass cover, and a separate condenser. A vertical steel reflector fitted in the top part of the evaporator cast a shadow over the condenser system. It was found that the solar still with a condenser performed better than the one which had no condenser. It should be noted that the designs examined in all these studies are simple, and require simple skills and

materials to construct. However, the condenser unit is located in the shadow zone of the still (without a solar radiation shield), which exposes the condensing cover to diffuse and ground-reflected solar radiation components. Moreover, the sun is overhead and on either side of the latitude at a tropical site, thereby allowing the global solar radiation to reach and heat the bare condensing cover, and significantly reduce the cover-water temperature difference. This would adversely affect the thermal efficiency of the still. Consequently, there is limitation of time and space to the application of a solar distillation system with an unshielded separate condensing cover.

In the present work, a single-slope passive solar still with an external condenser has been studied theoretically. The performance of both the present solar still (PSS) and CSS was simulated under similar meteorological conditions. Simulation results are presented and discussed in this paper.

2. System description and modeling

A solar still with separate evaporator and condenser chambers has been studied numerically. The major components of the system are a) a horizontal basin 1 with saline water in the evaporator chamber (first effect), b) basin 2 with saline water (second effect), c) basin 3 with saline water (third effect), d) condensing cover and e) opaque insulation shield over the condensing cover (Fig.1a). Both basins 2 and 3 are located in the condenser.. The evaporator is covered with glass on the top part to enable solar radiation reach the saline water in the evaporator (Fig.1b). Water vapor from the evaporation basin

rises up and condenses on the inner side of the glass while part of the vapor flows into the condensing chamber by purging and diffusion where it condenses on the outer surface of the middle basin liner, thereby recovering part of the heat from the first effect. There is a condensing cover directly above the upper basin, with an inclined air channel (with a single open end) over the cover for cooling. The condensing cover is shielded from solar radiation by an opaque insulation cover, which forms part of the air channel. Distillate is collected by drainage channels on the bottom lower parts of the glass cover, middle basin liner, upper basin liner and condensing cover.

A mathematical model was developed to simulate the performance of the CSS and PSS under the same meteorological conditions (with γ=180^o). It was assumed that:

a) the two solar stills are air-tight,

b) purging and diffusion stop when the temperature of water in the middle basin exceeds that of the lower basin, and

c) ground-reflected solar radiation does not reach saline water in the evaporator basin.

With these assumptions, the heat balance equations for the present solar still components are as follows:

Glass cover (gc)

$$m_{gc}C_{p,gc}\frac{dT_{gc}}{dt}=A_{gc}F_{gc}G_{ef}+A_{w1}h_{gc}\left(T_{w1}-T_{gc}\right)-A_{gc}h_{c,gc\text{-}a}\left(T_{gc}-T_{a}\right)-A_{gc}h_{r,gc\text{-}sk}\left(T_{gc}-T_{sk}\right) \quad (1)$$

$$h_{gc}=\left(\frac{Rh_{c,w1-gc}}{1+R}+\frac{Rh_{e,w1-gc}}{1+R}+h_{r,w1-gc}\right) \quad (2)$$

Basin liner 1 (bl)

$$m_{b1}C_{p,b1}\frac{dT_{b1}}{dt}=A_{w1}\{F_{b1}G_{ef}-h_{c,b1-w1}(T_{b1}-T_{w1})-U_{bo}(T_{b1}-T_a)\} \quad (3)$$

Water in basin 1 (wl)

$$m_{w1}C_{P,w1}\frac{dT_{w1}}{dt}=A_{w1}\left[F_{w1}G_{ef}+h_{c,b1-w1}(T_{b1}-T_{w1})\right]-\dot{m}_d H_{w1}-A_{w1}h_{w1}(T_{w1}-T_{gc})-A_{s1}U_{sw}(T_{w1}-T_a) \quad (4)$$

$$h_{w1}=h_{c,w1-gc}+h_{e,w1-gc}+h_{r,w1-gc} \quad (5)$$

$$\dot{m}_d=D(\mathrm{A_{ec}}/x_{ec})(\varphi_{ve}-\varphi_{vc}) \quad (6)$$

Basin liner 2 (b2)

$$m_{b2}C_{p,b2}\frac{dT_{b2}}{dt}=A_{w1}h_{pu}(T_{w1}-T_{gc})+\dot{m}_d H_{w1}-A_{b2}h_{c,b2-w2}(T_{b2}-T_{w2}) \quad (7)$$

$$h_{pu}=\frac{h_{c,w1-gc}}{1+R}+\frac{h_{e,w1-gc}}{1+R} \quad (8)$$

Water in basin 2 (w2)

$$m_{w2}C_{p,w2}\frac{dT_{w2}}{dt}=A_{b2}h_{c,b2-w2}(T_{b2}-T_{w2})-A_{w2}h_{w2}(T_{w2}-T_{b3})-A_{s2}U_{sw}(T_{w2}-T_a) \quad (9)$$

$$h_{w2}=h_{c,w2-b3}+h_{e,w2-b3}+h_{r,w2-b3} \quad (10)$$

Basin liner 3 (b3)

$$m_{w3}C_{p,b3}\frac{dT_{b3}}{dt}=A_{w2}h_{w2}(T_{w2}-T_{b3})-A_{b3}h_{c,b3-w3}(T_{b3}-T_{w3}) \quad (11)$$

Water in basin 3 (w3)

$$m_{b3}C_{p,w3}\frac{dT_{w3}}{dt}=A_{b3}h_{c,b3-w3}(T_{b3}-T_{w3})-A_{w3}h_{w3}(T_{w3}-T_{co})-A_{s3}U_{sw}(T_{w3}-T_a) \quad (12)$$

$$h_{w3}=h_{c,w3-co}+h_{e,w3-co}+h_{r,w3-co} \quad (13)$$

Rate of evaporation ($\dot{m}_e$)

$$\dot{m}_e = \frac{h_{e,w1-gc}\left(T_{w1} - T_{gc}\right)}{H_{w1}} + \frac{A_{w2}h_{e,w2-b3}\left(T_{w2} - T_{b3}\right)}{A_{w1}H_{w2}} + \frac{A_{w3}h_{e,w3-co}\left(T_{w3} - T_{co}\right)}{A_{w1}H_{w3}} + \frac{\dot{m}_d}{A_{w1}} \tag{14}$$

The heat flux (Q_e) due to evaporation can be written as:

$$Q_e = h_{e,w1-gc}\left(T_{w1} - T_{gc}\right) + \frac{A_{w2}h_{e,w2-b3}\left(T_{w2} - T_{b2}\right)}{A_{w1}} + \frac{A_{w3}h_{e,w3-co}\left(T_{w3} - T_{co}\right)}{A_{w1}} + \frac{\dot{m}_d H_{w1}}{A_{w1}} \tag{15}$$

The distillate yield (m_{dw}) and efficiency of the system (η) in a time interval of (t_2-t_1) are calculated from:

$$m_{dw} = \int_{t_1}^{t_2} \dot{m}_e dt \tag{16}$$

$$\eta = \frac{100\int_{t_1}^{t_2} Q_e dt}{\int_{t_1}^{t_2} G_{gh} dt} \tag{17}$$

It should be mentioned that the heat balance equations for the CSS are similar to those of the components of the evaporator unit of the PSS with the following modifications:

Glass cover (gc)

$$h_{gc} = h_{c,w1-gc} + h_{e,w1-gc} + h_{r,w1-gc} \tag{18}$$

Water in basin (w1)

$$\dot{m}_d = 0 \tag{19}$$

Rate of evaporation ($\dot{m}_e$)

$$\dot{m}_e = h_{e,w1-gc}\left(T_{w1} - T_{gc}\right) / H_{w1} \tag{20}$$

The values of the solar absorption factor F were computed as follows [12]:

$$F_{gc}= \alpha_{gc} \quad (21)$$

$$F_{wl} =\alpha_{wl} (1- \alpha_{gc} - \rho_{gc}) \quad (22)$$

$$F_{bl} =\alpha_{bl}[1-\alpha_{gc}-\rho_{gc}-\rho_{wl} (1-\alpha_{gc}-\rho_{gc})- F_{wl}] \quad (23)$$

Physical properties used in the present study are: $C_{p,gc}$=750 J kg^{-1} K^{-1}, $C_{p,bl}= C_{p,b2} = C_{p,b3}$ =477 J$kg^{-1}K^{-1}$, α_{wl}=0.05, ρ_{wl}=0, ρ_{bw}=0.05, ε_{gc}=0.88, ε_{w}=0.96 and ε_{co}=0.80. At normal incidence, the values of α_{gc} and ρ_{gc} were taken to be 0.10 and 0.12 respectively. It was assumed that the condensing cover and the basin liner were made of galvanized iron sheet while the solar shield was made of plywood. A temperature-dependent correlation was used to calculate the specific latent heat of water vaporization [13]. The saturation vapor pressure inside the solar still was calculated using a correlation reported by ASHRAE [14], and other physical properties of water (k,α', β', ν and ρ) were computed from temperature-dependent correlations [15]. The densities of water vapor in the evaporator (φ_{ve}) and condenser (φ_{vc}) chambers were calculated using Eq.(24), at 0.5(T_{wl}+T_{gc}) and 0.5(T_{b2}+T_a) respectively. The reference design, operational and meteorological parameters for both the CSS and PSS are presented in Table 1.

$$\varphi=P/(R_vT) \quad (24)$$

Heat loss from the top of the glass cover to the environment is predominantly by convection (to ambient air) and radiation (to sky). Wind influences the convective heat transfer from the top part and the wind coefficient of heat transfer is calculated from [16]:

$$h_{c,gc-a} = \begin{cases} 2.8 + 3V_{wd}, V_{wd} \le 5ms^{-1} \\ 6.15V_{wd}^{0.8}, V_{wd} > 5ms^{-1} \end{cases} \quad (25)$$

The coefficient of radiative heat transfer to the sky is given by [12]:

$$h_{r,gc-sk} = \sigma \varepsilon_{gc} (T_{gc}^2 + T_{sk}^2)(T_{gc} + T_{sk}) \tag{26}$$

with the following correlation for sky temperature [17]:

$$T_{sk} = 0.0552\, T_a^{1.5} \tag{27}$$

The evaporation and condensation processes involve the transfer of both heat and mass. Consequently, relevant correlations are used to estimate the coefficients of internal convective and evaporative heat transfers from hot water to each of the condensing surfaces [18]:

$$h_{c,w-cs} = 0.884\left[(T_w - T_{cs}) + \frac{(P_w - P_{cs})T_w}{268900 - P_w} \right]^{1/3} \tag{28}$$

$$h_{e,w-cs} = \frac{0.016273 h_{c,w-cs} (P_w - P_{cs})}{T_w - T_{cs}} \tag{29}$$

In addition, there is internal heat radiation from hot water to each of the condensing surfaces. The coefficient of internal radiative heat transfer is estimated from [12]:

$$h_{r,w-cs} = \sigma \varepsilon_{w,cs} (T_w^2 + T_{cs}^2)(T_w + T_{cs}) \tag{30}$$

$$\varepsilon_{w,cs} = \left(\frac{1}{\varepsilon_w} + \frac{1}{\varepsilon_{cs}} - 1 \right)^{-1} \tag{31}$$

The coefficient of convective heat transfer from the middle and upper basin liners to saline water is calculated according to Incropera and Dewitt [19], assuming the basins are inclined to the horizontal:

$$h_c = Nu\ k/S \tag{32}$$

$$Nu = \left\{ \frac{0.825 + 0.387\ Ra^{1/6}}{\left[1 + (0.492/\mathrm{Pr})^{9/6}\right]^{8/27}} \right\}^2 \tag{33}$$

$$Pr = C_p \nu / k \tag{34}$$

$$Ra = \frac{g\beta' S^3 (\Delta T) \sin\beta}{\alpha' \nu} \tag{35}$$

$$S = A/(2L + 2B) \tag{36}$$

In addition, there is heat loss from the bottom and side walls of the still. In this study, the coefficient of bottom heat loss is calculated from [12]:

$$U_{bo} = \left(\frac{x_1}{k_1} + \frac{x_2}{k_2} \right)^{-1} \tag{37}$$

with the coefficient of heat loss from the sides estimated from:

$$U_{sw} = \frac{k_2}{x_2} \tag{38}$$

Several authors have reported constant values of the coefficient of convective heat transfer from the evaporator basin liner to saline water in the basin ($h_{c,b1\text{-}w1}$). Mowla and Karimi [20] used a value of 130 W m^{-2} K^{-1} while Zurigat and Abu-Arabi [21] chose a value of 135 W m^{-2} K^{-1}. Tripathi and Tiwari [22] reported $h_{c,b1\text{-}w1}$ = 100 Wm^{-2} K^{-1}. A value of 100 Wm^{-2} K^{-1} worked well in the present study.

3. Solution procedure

The performance of the present still was simulated together with a conventional system (with the same corresponding design parameters) under similar operating and meteorological conditions, and using hourly horizontal global (I_{gh}) solar radiation data from Chileka weather site (15° 40′ S, 34° 58′ E) in Malawi. Solar radiation data at intervals shorter than one hour is not available in Malawi and, therefore, mean values were

calculated from the hourly totals to obtain global irradiance (G_{gh}) on a horizontal surface. The solar climate of Malawi is reported elsewhere [23, 24].

$$G_{gh}=I/3600 \tag{39}$$

Incoming solar radiation is incident on the glass cover and part of it is directly transmitted onto the surface of saline water in the evaporator basin (Fig.1b). In addition, the walls of the evaporator chamber and the front wall of the condenser chamber reflect solar radiation onto the water surface, and they cast shadows over the water surface during certain times of the day. In view of this, effective solar irradiance (G_{ef}) inside the solar still is used in the heat balance equations [25]. Solar energy available on the back, eastern side and western side walls of the evaporator chamber, and the front wall of the condenser chamber are included in the computation of $G_{ef.}$. It is also assumed that the front wall of the evaporator chamber contributes a negligible proportion of the solar energy that reaches the surface of water, and the solar energy received by saline water in the evaporator basin can be given by [25]:

$$A_{wl}G_{ef} = A_{sb}G_{gh} + (\rho_{iw}A'_{iw} + \rho_{fc}A'_{fc})G_{gh} \tag{40}$$

$$A'_{iw} = A'_{bw} + A'_{ew} + A'_{ww} \tag{41}$$

$A_{sb}G_{gh}$ is the solar energy received by the water directly while the remainder is reflected from the walls of the solar still (Eq.40). Solar energy available on the walls (G_{wa}) is:

$$G_{wa} = A'_{iw}G_{gh} + A'_{fc}G_{gh} \tag{42}$$

The area of saline water receiving solar radiation directly and the total projected area of the walls are computed from the solar altitude and azimuth angles, and latitude and longitude of the site. At a given time of the day, the solar altitude and azimuth angles are

calculated according to Duffie and Beckman [12]. The area of water receiving solar radiation directly, and projected areas of the back, eastern side, west and front condenser walls are calculated by using the geometrical analysis of Fig.2. The area of water receiving solar radiation directly (A_{sb}) is computed as follows:

Area of rectangle AIK′X, $A_1 = \left(L_{b1} - \frac{Z_{fe} \sin(|\gamma_s - \gamma|)}{\tan\psi} \right) \frac{Z_{fe} \cos(\gamma_s - \gamma)}{\tan\psi}$ (43)

Area of rectangle BCHX, $A_2 = \frac{B_{b1} Z_{fe} \cos(\gamma_s - \gamma)}{\tan\psi}$ (44)

Area of triangle GHK′, $A_3 = 0.5 \left(B_{b1} - \frac{Z_{fe} \cos(\gamma_s - \gamma)}{\tan\psi} \right)^2 \tan r$ (45)

$$\sin r = \frac{(Z_{bw} - Z_{fe}) \sin(|\gamma_s - \gamma|)}{\left[(B_{b1} \tan\psi)^2 + (Z_{bw} - Z_{fe})^2 + 2B_{b1} (Z_{bw} - Z_{fe}) \tan\psi \cos(\gamma_s - \gamma) \right]^{0.5}} \quad (46)$$

$A_{sb}=L_{bl}B_{bl} - (A_1+A_2+A_3)$ (47)

The projected areas of the back wall of the evaporator chamber and front wall of the condenser chamber are calculated from [25]:

$$A'_{bw} = \frac{L_{b1} Z_{bw} \cos(\gamma_s - \gamma)}{\tan\psi} \quad (48)$$

$$A'_{fc} = \frac{L_{b1} Z_{fc} \cos(\gamma_s - \gamma)}{\tan\psi} \quad (49)$$

In the morning (ω<0), rays of the sun are incident on the outer surface of the east wall and on the inner surface of the west wall. At solar noon (ω=0), both the east and west walls receive equal amounts of solar energy. In the afternoon (ω>0), the trend in the distribution

of solar energy on the east and west walls is reversed. In view of the symmetry about solar noon, the projected areas of the two walls are given by:

$$A'_{ew} = \begin{cases} B_{b1}\left[\dfrac{Z_{fe}\sin(|\gamma_s - \gamma|)}{\tan\psi} + 0.5y\sin r\right], \omega \geq 0 \\ 0, \omega < 0 \end{cases} \quad (50)$$

$$A'_{ww} = \begin{cases} B_{b1}\left[\dfrac{Z_{fe}\sin(|\gamma_s - \gamma|)}{\tan\psi} + 0.5y\sin r\right], \omega \leq 0 \\ 0, \omega > 0 \end{cases} \quad (51)$$

$$y = \left[B_{b1}^2 + \left(\frac{Z_{bw}}{\tan\psi} - \frac{Z_{fe}}{\tan\psi}\right)^2 + 2B_{b1}\left(\frac{Z_{bw}}{\tan\psi} - \frac{Z_{fe}}{\tan\psi}\right)\cos(\gamma_s - \gamma)\right]^{0.5} \quad (52)$$

In addition, hourly ambient air temperature was estimated from daily minimum and maximum ambient temperatures [26]. Similar equations were used to compute the effective solar irradiance in the CSS, with Z_{fc}=0.

A computer program was written in MATLAB to solve the above system of non-linear equations using the Gauss-Seidel iterative method [27], with a temperature tolerance of 0.5 K and time step of 20 s. The temperature of the condensing cover (T_{co}) was assumed equal to ambient air temperature (T_a), [9]. Initial values of the temperatures of the system components were assumed to be approximately equal to T_a. Based on these values of temperature and physical properties, appropriate coefficients of heat transfer (assumed constant in a given time step) were calculated for estimating temperatures in the next time step. The flow chart of the program is presented in Fig.3.

4. Results

41 Irradiance and temperature variation

Fig.4 shows the variation of observed and effective global irradiance with time. It is seen that the observed irradiance is higher than the effective irradiance in both the CSS and PSS, probably because some of the solar radiation intercepted by the glass cover does not reach the surface of saline water. Nevertheless, the effective irradiance in the PSS is slightly higher than that in the CSS, maybe due to the contribution of solar energy from the front wall of the condenser chamber for the PSS. Moreover, solar radiation is the most influential environmental parameter in distillate productivity [28]. These observations indicate that the direct use of G_{gh} in the heat balance equations would lead to overestimation of the distillate yield.

Fig.5 shows the variation of the temperature of the ambient air (T_a), glass cover (T_{gc}), and water in basins 1 (T_{w1}), 2 (T_{w2}) and 3 (T_{w3}) at reference values of the design, operating and meteorological parameters. It is observed that all the temperatures conform to the variation in irradiance on the sample day. The values of T_{gc} for the CSS are higher than those of the PSS. At 12:00 h, the temperature difference (T_{w1}-T_{gc}) is 9 and 14 K for the CSS and PSS respectively. This is probably due to heat flow from the evaporator basin into the condenser chamber which tends to lower the glazing temperature, thereby increasing (T_{w1}-T_{gc}) in the PSS.

The temperature of saline water (T_{w1}) in the evaporator basin of the CSS is higher than that in the evaporator basin of the PSS during the most part of the day, with the difference (11 K) being maximum around 14:00 h. This trend is attributed to the heat transfer modes from water in the evaporator basins (first effect) of the systems. In the conventional solar

still, heat is lost to ambient environment through the glass cover, bottom and side walls while heat is transferred by purging (predominantly) and diffusion from the evaporator basin to the condenser unit of the PSS, in addition to heat loses through the glass cover, bottom and side walls. It is nevertheless pleasing to note that the values of T_{wl} are comparable with experimental data reported in literature [11, 29].

It is also seen that the temperature of water (T_{w2}) in basin 2 (second effect) is below that of basin 1 of the present solar still from morning 8:00 h to around 17:00 h). This indicates that water vapor from the evaporator is able to condense on the underside of the basin 2 during the most part of the day, thereby augmenting the rate of productivity. After sunset, the temperature of the water in the basin 2 is higher than that of basin 1 probably due to lower rate of top heat loss from basin 3 than that from the glazing cover. The latter component of the solar still loses heat to environment through convection and radiation while water in the upper basin loses heat to the condenser cover which has an insulation shield over it. So, top heat loss from the condenser cover is predominantly by natural convection which would account for the lower rate of cooling in basins 2 and 3.

The temperature of water in basin 3 (T_{w3}) is lower than that of water in basin 2 (T_{w2}) of the PSS from 9:00 h to later than 24:00 h, which again shows that vapor from water in basin 2 would be able to condense on the underside of basin 3 during the most part of the day. In addition, T_{w3} is higher than T_a from 11:00 h until after 24:00 h, which also indicates that distillate production would take place from the third effect during this period.

4.2 Distillate productivity

In this paper, the reported distillate productivity for the PSS is the total of contributions from water in the lower basin (first effect), middle basin (second effect) and upper basin

(third effect). Fig.6 shows the variation of cumulative distillate productivity of the CSS and PSS at reference values of the design, operating and meteorological parameters. It is seen that in the morning (up to about 10:00 h), the distillate productivity is extremely low for both stills. This is expected because production starts when air inside the still is saturated with water vapor. From about 10:00 h, the productivity of the CSS is lower than that of the PSS. At 24:00 h, the cumulative productivity of the CSS is 3.754 kg m^{-2} (with η=32 %) while that of the PSS is 6.080 kg m^{-2} (with η= 52 % and an improvement of 62 %). It should also be noted that there is insignificant production after 24:00 h. For the PSS, distillate contributions from the first, second and third effects are 60, 22 and 18 % respectively. Purging contributes 97 % the water vapor that condenses on the under side of the upper basin while diffusion accounts for the remaining proportion. The daily productivity of a CSS is about 3-4 kg m^{-2}, with a maximum thermal efficiency of 35 % [2, 30], which agree with the present observations. Results for the PSS also conform very well to experimental findings of El-Bahi and Inan [5] and Fath and Elsherbiny [9].

4.3 Sensitivity analysis

A sensitivity analysis of the solar still with a separate condenser is presented in this section (A parameter is varied while all the others are fixed at their respective reference levels). Fig.7 shows the variation of distillate productivity with the absorptance of the basin liner in the evaporator basin (α_{bl}). It is seen that productivity significantly increases with the magnitude of α_{bl}, consistent with results commonly reported in literature. For this reason, still basin liners (and other solar absorbing surfaces) are often painted black (or

other black thin film used) on the inner surface to enhance absorption of incoming solar radiation, which increases the water temperature and distillate yield.

Fig.8 shows the effect of the ratio (R) of the volume of the evaporator chamber to that of the condenser chamber. It is observed that the distillate productivity decreases with increasing values of R. This observation is attributed to the fact that the pressure of air increases with decreasing volume. So, as the volume of the evaporator decreases, the pressure in the evaporator also increases, which results in an increase in purging from the evaporator chamber into the condenser chamber. These results are consistent with findings of Fath [10].

The effect of the mass of water in the first (m_{wl}), second (m_{w2}) and third (m_{w3}) basins on the distillate productivity are presented in Fig.9. Productivity decreases by 0.980 kg m^{-2} when m_{wl} is increased from 10 to 30 kg, probably due to an increase in the thermal mass of water which results in low temperatures being attained by the water (for the same amount of solar radiation intercepted by the system).These results conform to well-known previous findings on the effect of m_{wl} on distillate productivity. Productivity decreases by 0.612 kg m^{-2} when m_{w2} is increased from 10 to 30 kg, and by 0.144 kg m^{-2} when m_{w3} is increased from 10 to 30 kg. It is observed that the effect of m_{w2} on productivity is more significant than that of m_{w3}.

The effect of wind speed (V_{wd}) on distillate production is shown in Fig.10. It is observed that the levels of production for three different wind speeds are not significantly different from morning (6:00 h) to about 15:00 h. After 15:00 h, the cumulative distillate is highest for V_{wd} =2 m s^{-1} and lowest for V_{wd}= 6 m s^{-1}. El-Sebaii [31] found that still productivity decreased with increasing V_{wd} until a typical wind velocity was reached, for saline water

masses (m_{wl}) less than 45 kg m^{-2}. Our present findings are therefore reasonable because m_{wl}=20 kg m^{-2}.

A summary of the sensitivity analysis is presented in Table 2. It is observed that the PSS is sensitive to absorptance of the evaporator basin liner (α_{bl}), ratio of the evaporator to condenser chamber volumes (R), mass of water in the evaporator basin (m_{wl}), mass of water in the middle basin (m_{w2}) and wind velocity (V_{wd}). However, the mass of water in the upper basin (m_{w3}) marginally affects the performance of the still.

4.4 Model performance

Simulation results show that the temperatures of the various still components are high during day time and low at night or during periods of low irradiance, which is expected in reality. In addition, the range of values of temperature is consistent with experimental results reported in literature. It is also observed that the levels of distilled water produced by the two solar stills also compare favorably with findings from previous studies. It appears therefore that the performance of our model is satisfactory.

5. Conclusion

A passive solar still with separate condenser has been studied theoretically. The system has one basin in the evaporation chamber (basin 1) and two basins (2 and 3) in the condenser chamber. The top part of the condenser is shielded from solar radiation. This solar still can be constructed using simple materials and skills, and applied without limitation to location and season. The performance of the present system is evaluated and

compared with that of a conventional solar still under the same meteorological conditions. Results show that the distillate yield of the present still is higher than that of the conventional type under the same meteorological conditions. Purging is the most significant mode of vapor transfer from the evaporator into the condenser chamber, while the first effect contributes the highest proportion to the total distillate yield. It is also found that the productivity of the solar still with separate condenser is most sensitive to the absorptance of the evaporator basin liner, mass of water in basins 1 and 2, and wind velocity. The mass of water in basin 3 has a marginal effect on distillate production. The performance of the present solar still is satisfactory.

Nomenclature

A area (m^2)

A_{ec} area across the entrance from the evaporator to condenser chamber (m^2)

A' projected area (m^2)

B width (m)

C_p specific heat capacity at constant pressure ($J\ kg^{-1}\ K^{-1}$)

CSS conventional solar still

D coefficient of diffusion mass transfer of water vapor in air ($=2.56x10^{-5}\ m^2\ s^{-1}$)

g acceleration due to gravity ($m\ s^{-2}$)

F solar radiation absorption factor (dimensionless)

G irradiance (Wm^{-2})

h coefficient of heat transfer ($W\ m^{-2}\ K^{-1}$)

H specific latent heat of vaporization ($J\ kg^{-1}$)

I hourly insolation ($J\ m^{-2}$)

k thermal conductivity (W m^{-1} K^{-1})

L length (m)

m mass (kg)

$\dot{m}$ rate of mass flow (kg s^{-1})

Nu Nusselt number (dimensionless)

P pressure (N m^{-2})

PSS present solar still

Pr Prandtl number (dimensionless)

Q heat flux (W m^{-2})

R ratio of evaporator chamber volume to condenser chamber volume (dimensionless)

Ra Rayleigh number (dimensionless)

R_v vapour gas constant (J $kg^{-1}K^{-1}$)

S channel or equivalent spacing (m)

t time (s)

T temperature (K)

U coefficient of heat loss (W m^{-2} K^{-1})

V velocity (m s^{-1})

x thickness (m)

x_{ec} gap crossed by water vapour from evaporator to condenser shown in Fig. (1), (m)

Z height (m)

Greek symbols

α absorptance (dimensionless)

α' thermal diffusivity ($m^2\ s^{-1}$)

β angle of inclination (degree)

β' coefficient thermal expansivity (K^{-1})

γ surface azimuth angle measured from the south (degree)

γ_s solar azimuth angle measured from the south (degree)

Δ change in

η system efficiency (%)

ρ reflectance (dimensionless)

τ transmittance (dimensionless)

φ density ($kg\ m^{-3}$)

σ Stefan-Boltzman constant ($W\ m^{-2}\ K^{-1}$)

ε emittance (dimensionless)

ν kinematic viscosity ($m^2\ s^{-1}$)

ω hour angle (degree)

Subscripts

1 initial/first

2 final/second

a air/ambient

bl-wl from basin liner 1 to water in basin 1

b2-w2 from basin liner 2 to water in basin 2

bo bottom

bw back wall of evaporator chamber

b3-w3	from basin liner 3 to water in basin3
c	convective
co	condensing cover
cs	condensing surface (glass cover, upper basin liner and condensing cover)
d	diffusion
dw	distilled water
e	evaporative
ef	effective
ew	eastern side wall
fc	front wall of the condenser chamber
fe	front wall of the evaporator chamber
gc	glass cover
gc-a	from glass cover to ambient air
gc-sk	from glass cover to sky
gh	global on horizontal surface
iw	internal part of the wall
pu	purging
r	radiative
sb	still base
sk	sky
sl	side wall around basin 1
s2	side wall around basin 2
s3	side wall around basin 3

sw side wall

vc vapor in condenser chamber

ve vapor in evaporator chamber

w water

wd wind

wl-gc from water in basin 1 to glass cover

w2-b3 from water in basin 2 to basin liner 3

w3-co from water in upper basin to condenser cover

ww western side wall

Acknowledgements

The authors are very grateful to the Commonwealth Scholarship Commission for the financial support. The Centre for WASHTED at the Malawi Polytechnic, and Universities of Strathclyde and Malawi are also acknowledged for the various forms of support.

References

[1] Abu-Qudias M, Bassam A, Abu-Hijleh K, Othman ON. Experimental study and Numerical simulation of a solar still using an external condenser. Energy 1996; 21: 851-855.

[2] Al-Kharabsheh S, Goswami DY. Experimental study of an innovative solar water desalination system utilizing a passive vacuum technique. Solar Energy 2003; 75: 395-401.

[3] Tiris Ç, Tiris M, Türe İE. Improvement of basin type solar still performance: Use of

various absorber materials and solar collector integration. Renewable Energy 1996; 9:758-61.

[4] Akash BA, Mohsen MS, Osta O, Elayan Y. Experimental evaluation of a single-basin solar still using different absorbing materials. Renewable Energy 1998; 14: 307-310.

[5] El-Bahi A, Inan D. Analysis of a parallel double glass solar still with separate condenser. Renewable Energy 1999; 17:509-21.

[6] Bassam A, Hijleh KA, Rabab'h HM. Experimental study of a solar still with sponge cubes in basin. Energy conversion and Management 2003; 44:1411-1418.

[7] Abdel-Rehim ZS, Lasheen A. Improving the performance of solar desalination systems. Renewable Energy 2005; 30:1955-71.

[8] Tiwari GN, Singh HN, Tripathi R. Present status of solar distillation. Solar Energy 2003; 75:367-73.

[9] Fath HES, Elsherbiny SM. Effect of adding a passive condenser on solar still performance. Energy Conversion and Management 1993; 34:63-72.

[10] Fath HES. High performance of a simple design, two effect solar distillation unit. Desalination 1996; 107:223-33.

[11] El-Bahi A, Inan D. A solar still with minimum inclination, coupled to an outside condenser. Desalination 1999; 123:79-83.

[12] Duffie JA, Beckman WA. Solar Engineering of Thermal Processes, 2nd ed. New York:Wiley Interscience, 1991.

[13] Belessiotis V, Voropoulos E, Delyannis E. Experimental and theoretical method for determination of the daily output of a still: input-output method. Desalination 1995;

100:99-104.

[14] ASHRAE. Fundamentals Handbook. Atlanta:American Society of Heating, Refrigerating And Air-Conditioning Engineers, 2001.

[15] IAPWS. The IAPWS Formulation 1995 for the thermodynamic properties of ordinary water substance for general and scientific use. International Association for the Properties of Water and Steam, 1996.

[16] Wattmuf JH, Charters WWS, Proctor D. Solar and wind induced external coefficients for solar collectors. Compless 1977; 2:56.

[17] Sharma VB, Mullick SC. Estimation of heat-transfer coefficients, the upward heat flow, and evaporation in a solar still. ASME Journal of Solar Engineering 1991; 113:36-41.

[18] Dunkle RV. Solar water distillation: the roof type still and a multiple effect diffusion still. International Development in Heat Transfer. International Heat Transfer Conference, University of Colorado 1961, pp.895-902 (part 5).

[19] Incropera FP, Dewitt DP. Fundamentals of heat and mass transfer, 5th ed. New York: John Wiley & Sons, 2002.

[20] Mowla D, Karimi G. Mathematical modeling of solar stills in Iran. Solar Energy 1995; 55:389-393.

[21] Zurigat YH, Abu-Arabi MK. Modelling and performance analysis of a regenerative solar desalination unit. Applied Thermal Engineering 2004; 24:1061-72.

[22] Tripathti R, Tiwari G.N. Thermal modeling of passive and active solar stills for different depths of water by using the concept of solar fraction. Solar Energy 2006; 80:956-967.

[23] Diabate´ L, Blanc Ph, Wald L. Solar climate in Africa. Solar Energy 2004; 76: 733–744.

[24] Madhlopa A. Solar radiation climate in Malawi. Solar Energy 2006; 80:1055-7.

[25] Tripathi R, Tiwari GN. Performance evaluation of solar still by using the concept of solar fraction. Desalination 2004; 169:69-80.

[26] Muneer T. Solar radiation & daylight models for the energy efficient design of buildings. Oxford: Reed Educational and Professional Publishing Ltd ; 1997, chapt.7.

[27] Burden RL, Faires JD. Numerical Analysis, 3rd ed. Boston: PWS Publishers; 1985, chapt. 8.

[28] Nafey AS, Abdelkader M, Abdelmotalip A, Mabrouk AA. Parameters affecting solar still productivity. Energy Conversion and Management 2000; 41: 1797-1809.

[29] Porta MA, Chargy N, Fernández JL. Extreme operating conditions in shallow still. Solar Energy 1997; 61:279-86.

[30] Kalogirou S. Survey of solar desalination systems and system selection. Energy 1997; 22:69-81.

[31] El-Sebaii AA. Effect of wind speed on active and passive solar stills. Energy Conversion and Management 2004; 45:1187-1204.

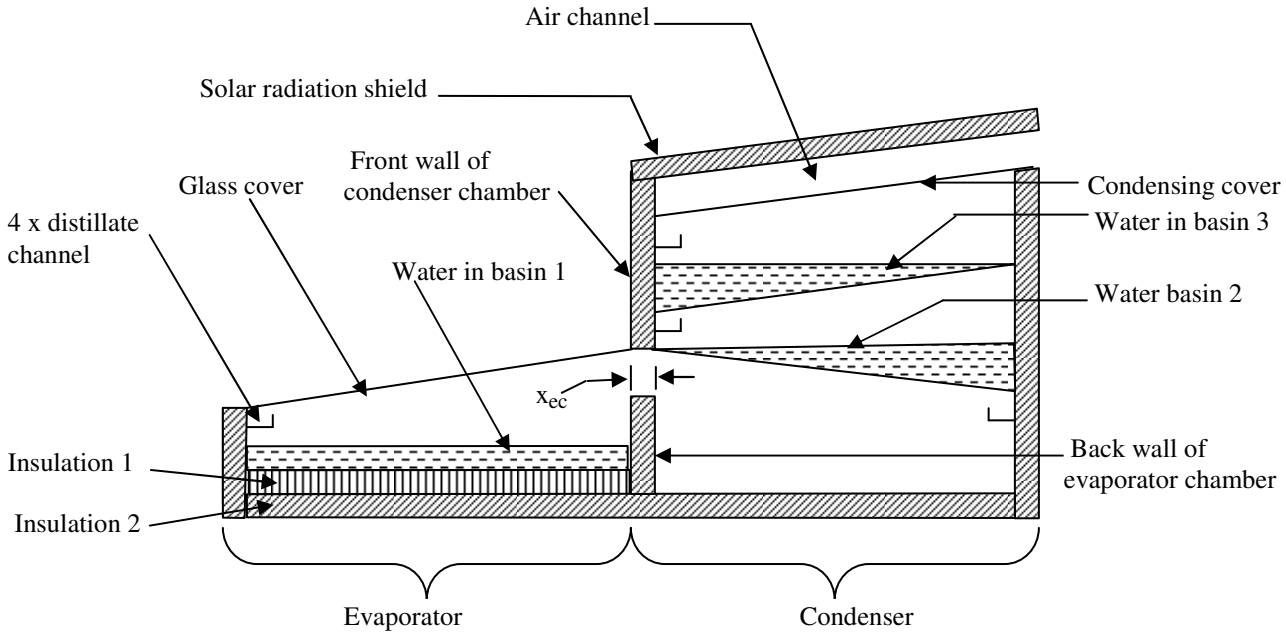
Air channel
Solar radiation shield
Front wall of condenser chamber
Glass cover
Condensing cover
4 x distillate channel
Water in basin 3
Water in basin 1
Water basin 2
x_{ec}
Insulation 1
Back wall of evaporator chamber
Insulation 2
Evaporator
Condenser

(a)

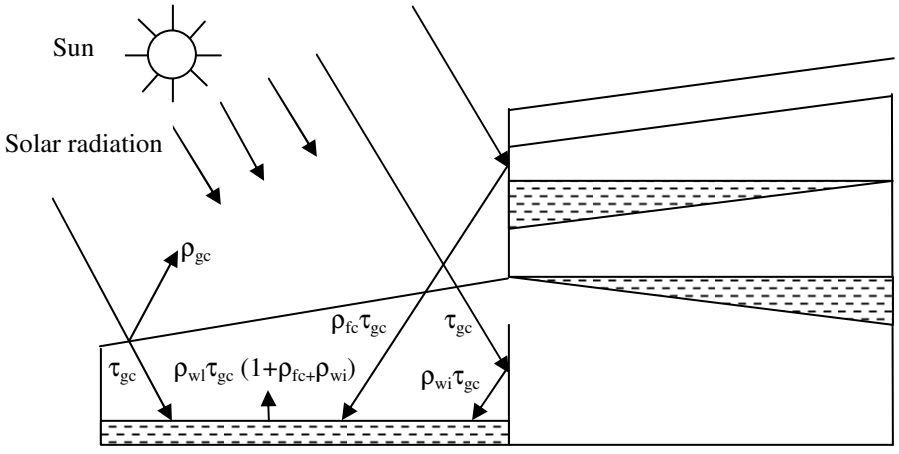
Sun
Solar radiation
ρ_{gc}
$\rho_{fc}\tau_{gc}$
τ_{gc}
τ_{gc}
$\rho_{wl}\tau_{gc}\ (1+\rho_{fc}+\rho_{wi})$
$\rho_{wi}\tau_{gc}$

(b)

Fig. 1: A cross-section of the present solar still, showing a) the evaporator and condenser units, and b) distribution of solar radiation inside the solar still.

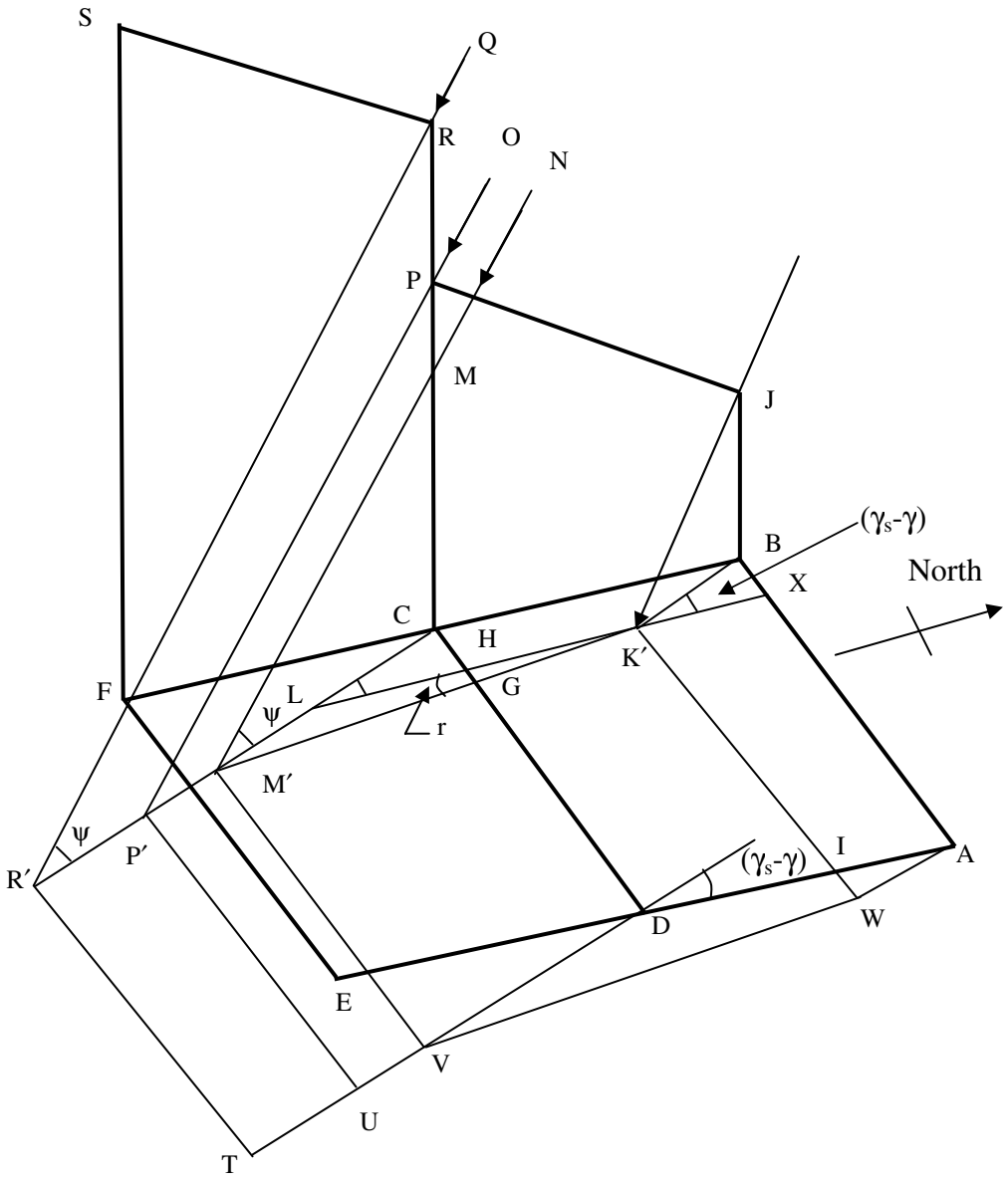

Fig.2: Geometry of the solar still and rays from the sun: ABFE= area of rectangular base of the still, ABCD=area of evaporator basin, BJPC=area of eastern side wall of the evaporator chamber, CFSR=area of eastern side wall of condenser chamber, AB=length of the evaporator basin (L_{bl}), AD= width of the evaporator basin (B_{bl}), LK′ is equal and parallel to BC, WK′ is equal and parallel to AB, BK′ is parallel and equal to CL, CM=height of back wall (Z_{bw}), angle BK′J=ψ, angle CLH=(γ_s-γ), BJ=height of front wall of evaporator basin (Z_{fe}), PR=height of the front wall of the condenser (Z_{fc}), CDVM′=projected area of the back wall, ADVW =projected area of west, TR′P′U=projected area of the front wall of the condenser chamber, DGK′I=area of water receiving solar radiation directly, and KK′, NM′, OP′and QR′ are sun rays projected on the still base.

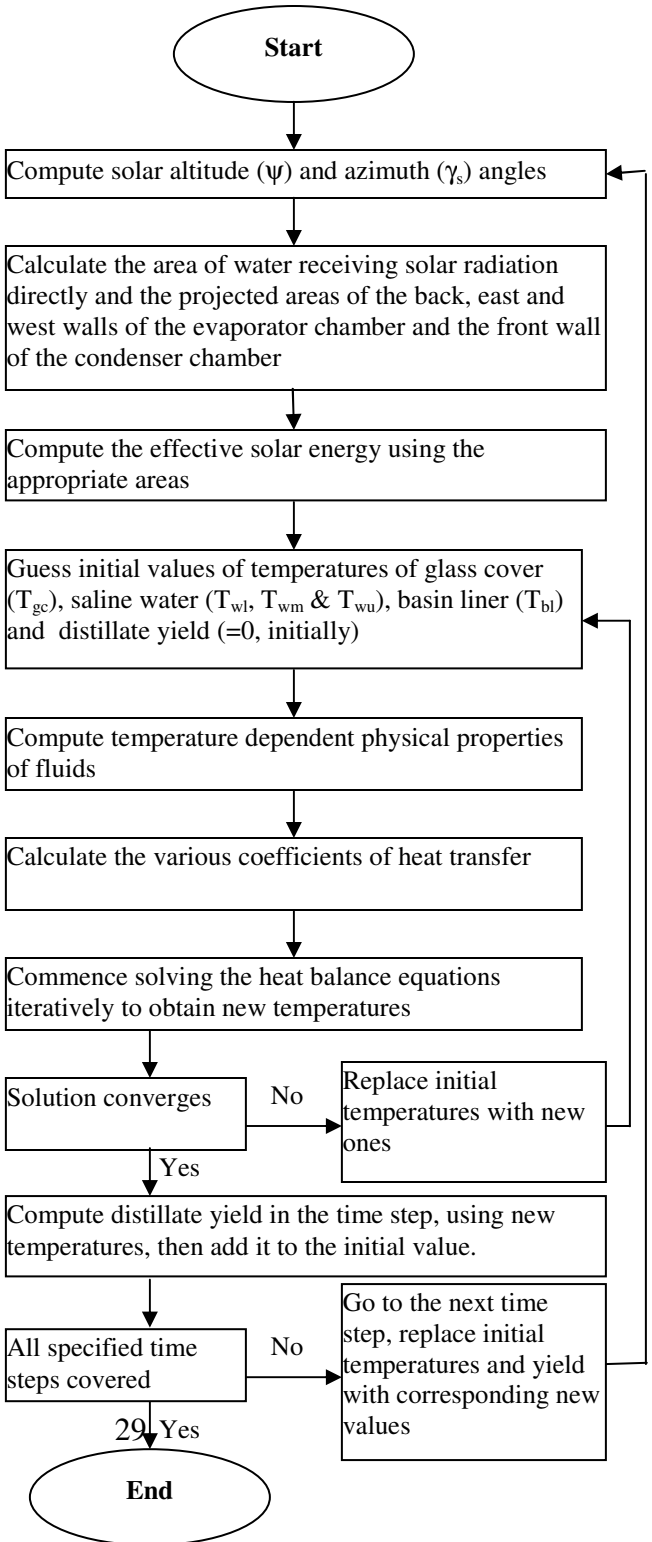

Fig.3: Flow chart for computation of the effective irradiance, temperatures of system components and distillate yield in MATLAB.

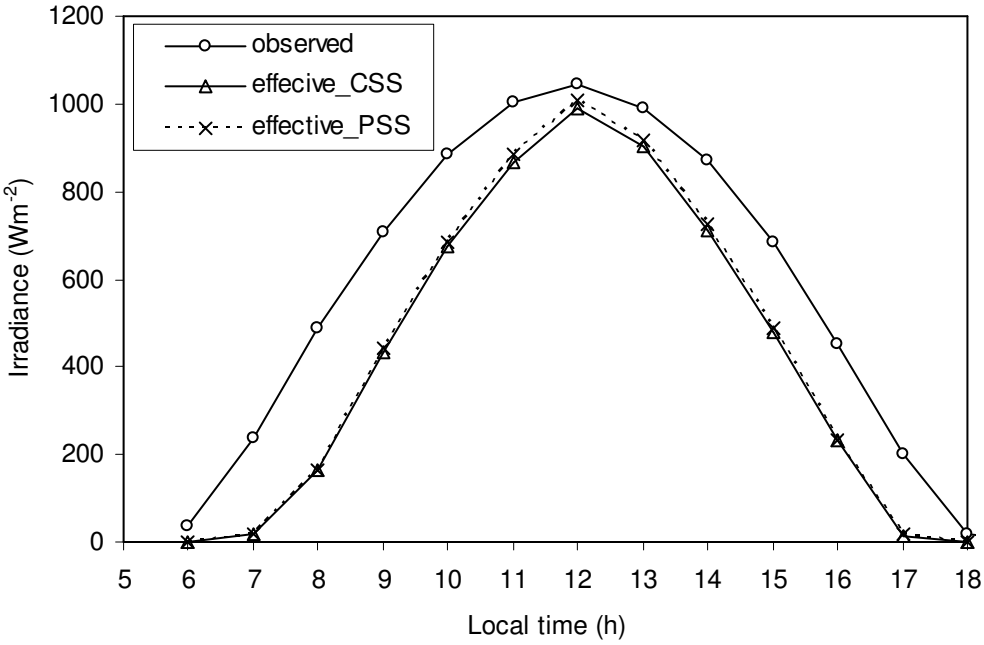

Fig.4: Variation of observed global irradiance, and effective irradiance in the conventional solar still (CSS) and present solar still (PSS).

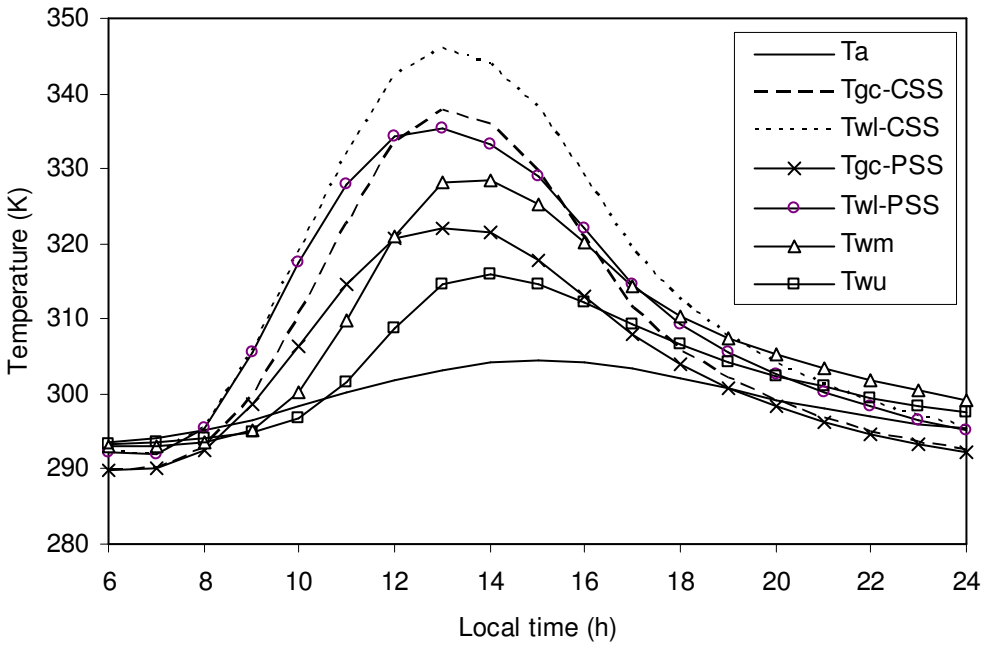

Fig.5: Variation of the temperature of ambient air(T_a), glass cover (T_{gc}), and water in the evaporator basin T_{wl}), middle basin (T_{wm}), and upper basin (T_{wu}) for the conventional solar still (CSS) and present solar still (PSS).

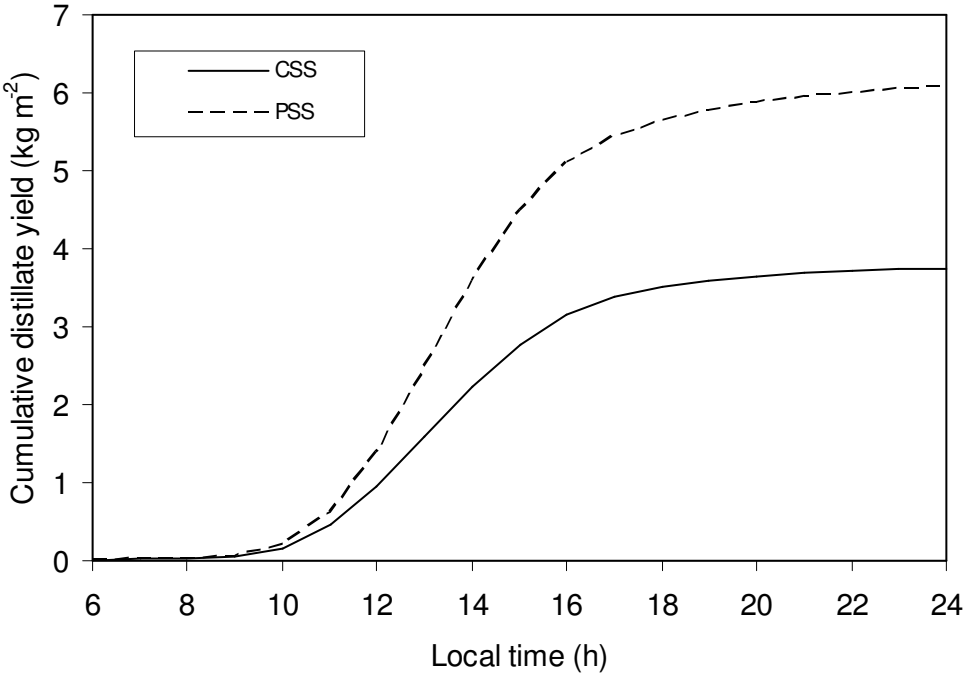

.Fig.6: Comparison of distillate yield for the conventional solar still (CSS) and present solar still (PSS).

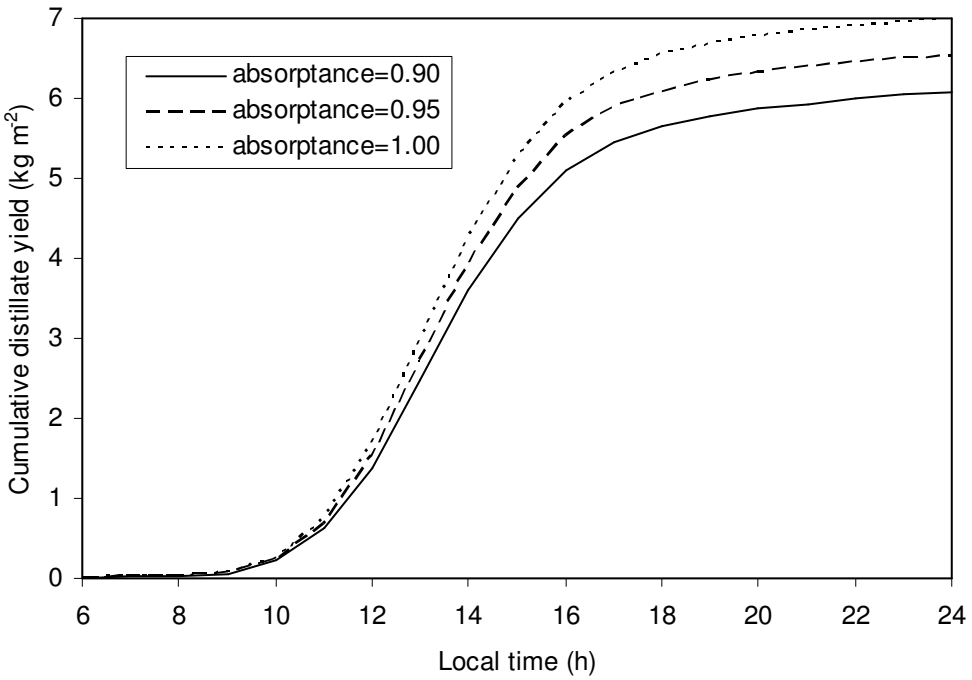

Fig.7: Effect of absorptance of the evaporator basin liner on distillate yield.

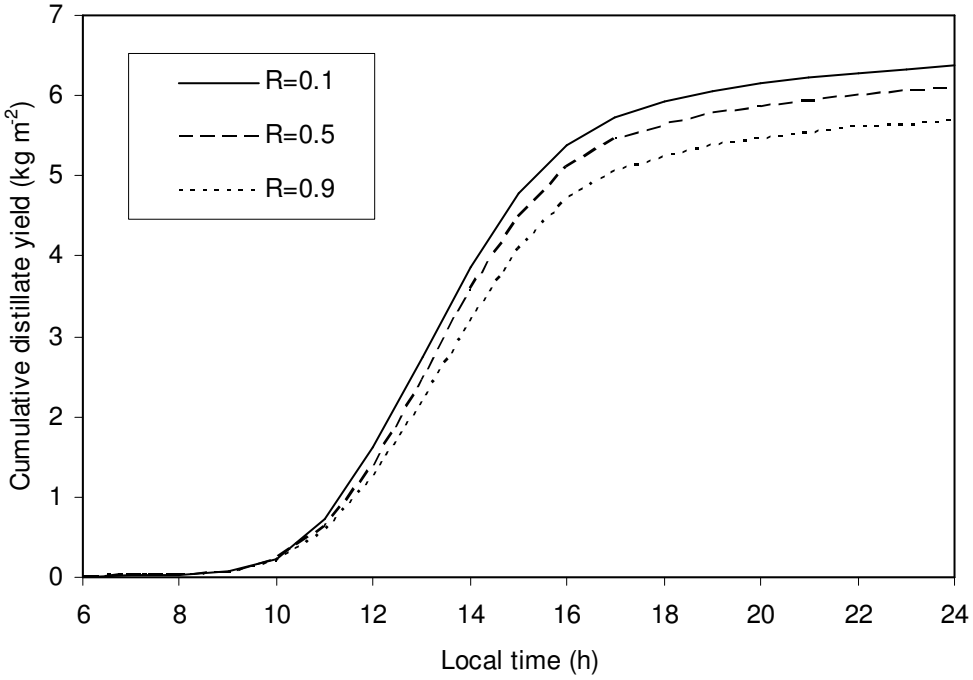

Fig.8: Effect of the ratio of the volume of the evaporator to condenser (R) on distillate yield.

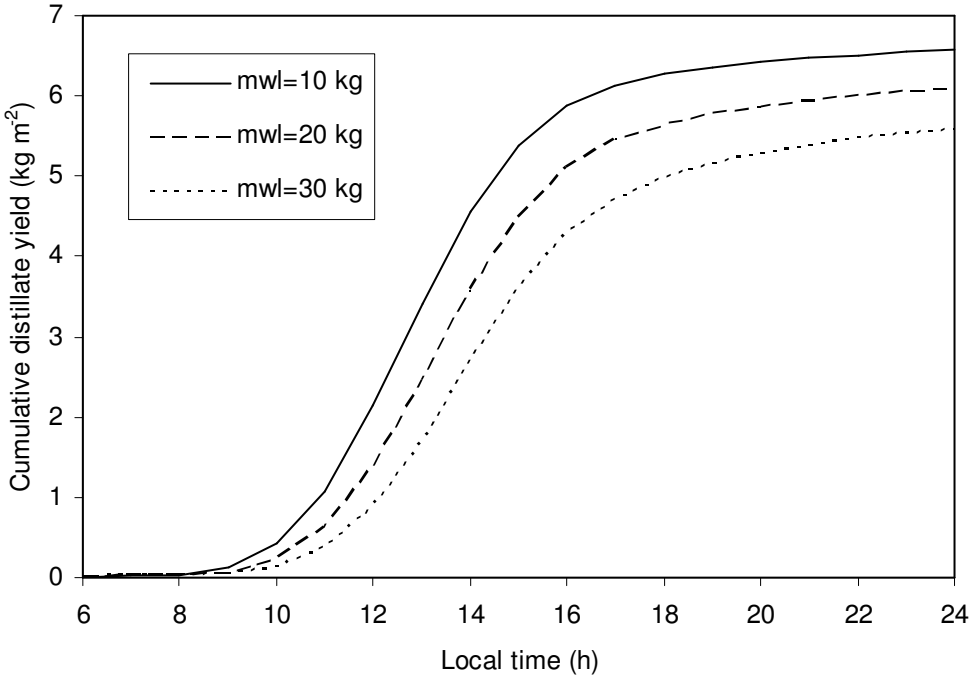
mwl=10 kg
mwl=20 kg
mwl=30 kg
Cumulative distillate yield (kg m-2)
Local time (h)
0
1
2
3
4
5
6
7
6
8
10
12
14
16
18
20
22
24

(a)

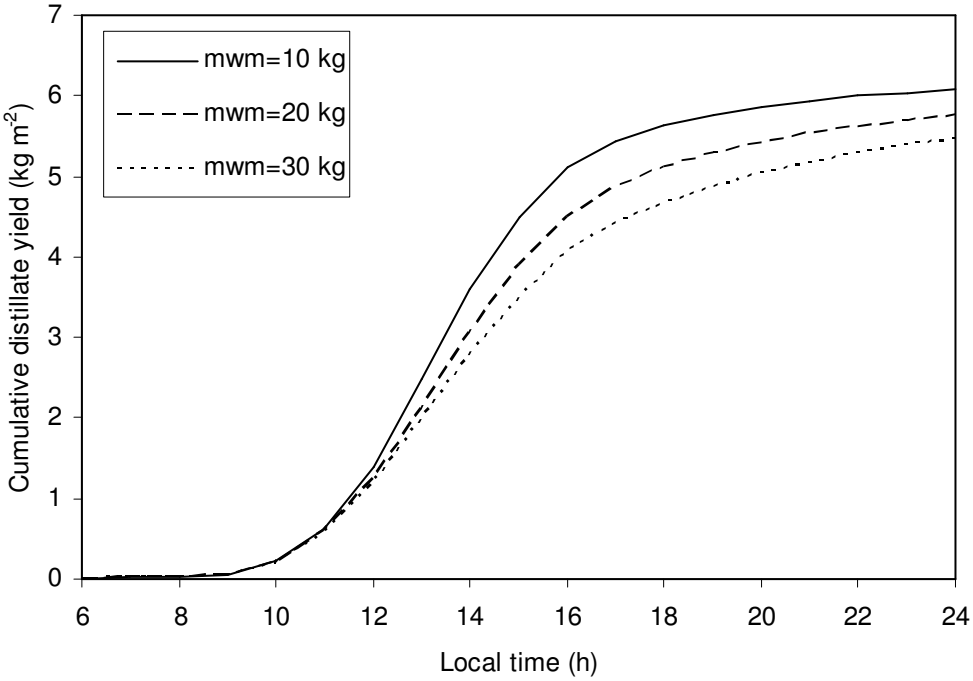
mwm=10 kg
mwm=20 kg
mwm=30 kg
Cumulative distillate yield (kg m-2)
Local time (h)
0
1
2
3
4
5
6
7
6
8
10
12
14
16
18
20
22
24

(b)

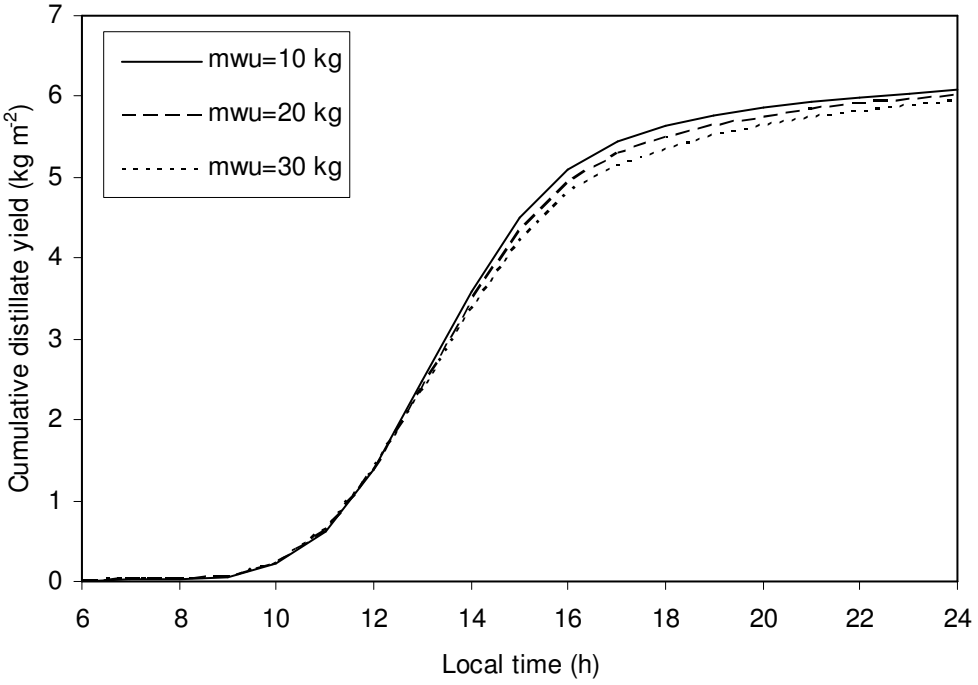

(c)

Fig.9: Effect of the mass of water in a) evaporator (m_{wl}), b) middle (m_{wm}) and c) upper (m_{wu}) basins on distillate productivity.

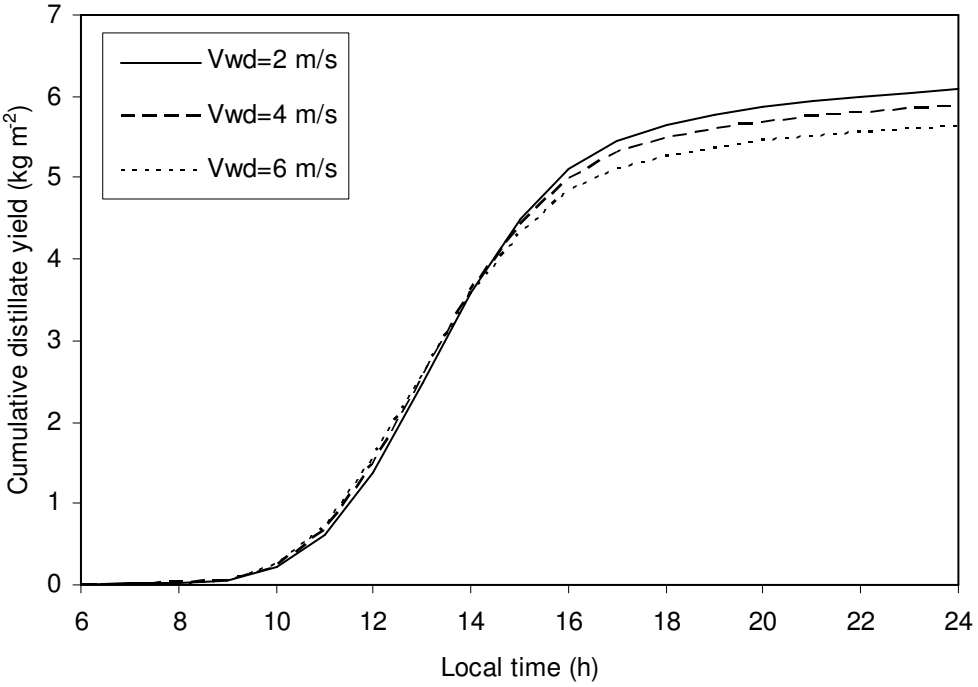

Fig.10: Effect of wind speed (V_{wd}) on the distillate productivity.

Table1: Reference design, operational and meteorological parameters for the conventional still (CSS) and present still (PSS).

Parameters	CSS	PSS
Design parameters		
A_{bl} (m^2)	1.000	1.000
A_{bu} (m^2)		1.015
A_{sc} (m^2)		0.05
A_{ev} (m^2)	1.262	2.606
A_{sm} (m^2)		1.294
A_{su} (m^2)		0.800
k_1 (W m^{-1} K^{-1})	0.0346	0.0346
k_2 (W m^{-1} K^{-1})	0.1200	0.1200
m_{bl} (kg)	5.0	5.0
m_{bu} (kg)		6.0
M_{bm} (kg)		6.0
m_{gc} (kg)	10	10
R (dimensionless)		0.5
x_1 (m)	0.020	0.020
x_2 (m)	0.023	0.023
x_{ec} (m)		0.02
Z_{bw}	0.468	0.418
Z_{fc}		0.632
Z_{fe}	0.238	0.238
α_{bl} (dimensionless)	0.95	0.95
β_{co} (degree)		10
β_{gc} (degree)	16	16
Operational parameters		
m_{wl} (kg)	20	20
m_{wm} (kg)	10	10
m_{wu} (kg)	10	10
Meteorological parameters		
V_{wd} (m s^{-1})	2	2

Table 2: Summary of the results of the effects of various parameters on distillate production.

Parameter	Range studied	Effect
M_{wl} (kg)	10-30	Sensitive
M_{wm} (kg)	10-30	Sensitive
M_{wu} (kg)	10-30	Marginally sensitive
R (dimensionless)	0.1 – 0.9	Sensitive
V_{wd} (m s^{-1})	2-6	Sensitive
α_{bl} (dimensionless)	0.90 – 1.00	Sensitive